Infrared Nano-Imaging of Dirac Magnetoexcitons in Graphene

Supplementary Information

S1. Magneto-Optical Conductivity Calculation

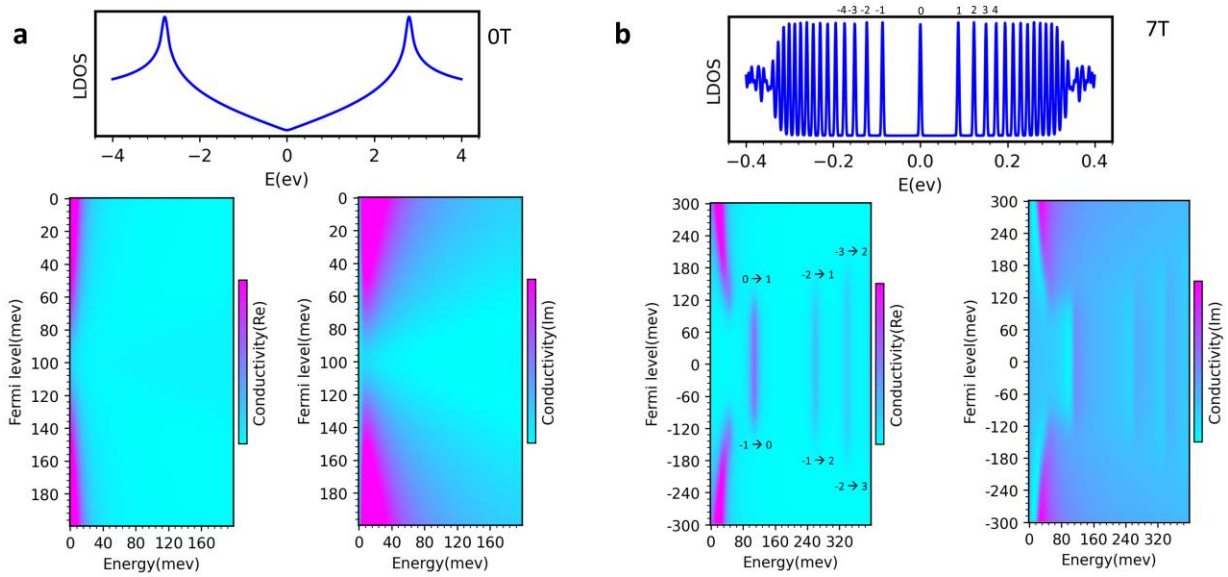

Fig.S2. *Local density of state (LDOS) of electrons (top) and 2D maps of the optical conductivity (bottom) of charge-neutral graphene at magnetic fields at 0 T (**a**) and 7 T (**b**).*

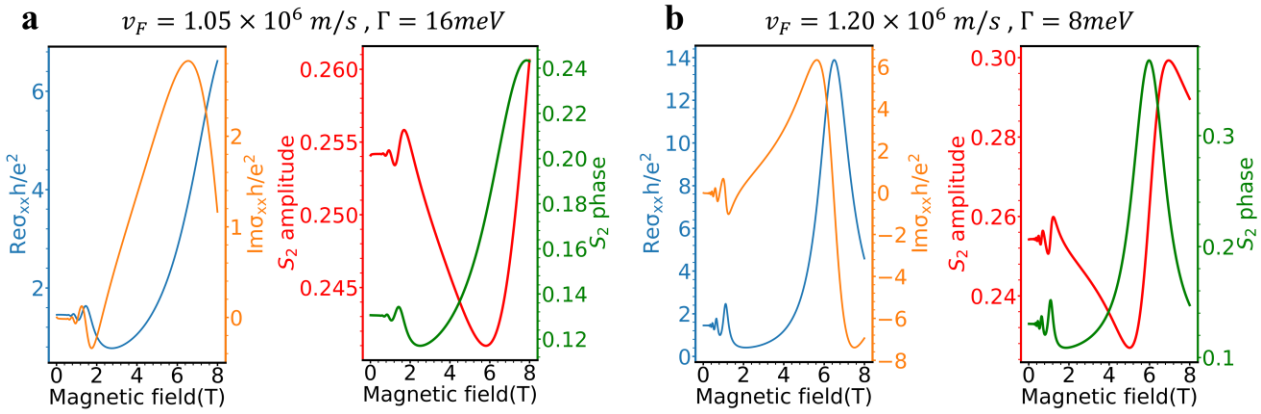

Fig.S3. *Magneto-optical conductivity (σ_{xx}) and near-field scattering signal (S_2) calculations at two different parameter sets, indicated at the top of **a** and **b**. v_F is the Fermi velocity and Γ is the scattering rate. The S_2 amplitude at 7T is higher for the higher v_F (the peak shifts to a lower magnetic field). The scattering rate determines the width of the peaks in σ_{xx} and S_2.*

The infrared magneto-optical conductivity in graphene is calculated based on Kubo formula and an energy-independent scattering rate approximation [4]. Similar approaches are used and agree well with the experimental results in both the terahertz and infrared frequency ranges [52–54].

The longitudinal conductivity of graphene in a magnetic field can be analytically expressed as

$$\sigma_{xx}(\omega) = i\frac{e^2}{2\pi}(\hbar\omega_c)^2 \times \sum_{n=0}^{\infty}\sum_{s=\pm1}\frac{\omega + i\Gamma}{E_{sn} - E_{n+1}}\frac{f(E_{sn}) - f(E_{n+1}) + f\left(E_{-(n+1)}\right) - f(E_{-sn})}{(E_{sn} - E_{n+1})^2 - (\omega + i\Gamma)^2} \quad \text{(S1)}$$

where Γ is the scattering rate, which determines the broadening of LL transitions and is assumed to be independent of frequency and LL index, $f(E_n) = \frac{1}{e^{(E_n-\mu)/k_BT}+1}$ is the Fermi-Dirac distribution function, and $E_n = \mathrm{sgn}(n)\sqrt{2|n|v_F^2|eB|/c}$ is the LL energy. The accuracy of the calculated magneto-optical conductivity is determined by the number of inter-Landau level transitions and a smaller magnetic field would require more LLs included in the calculation. A total of 80,000 LLs are included in the calculation and the formula reproduces the graphene conductivity in the low field limit in the energy range we considered in this work. The calculated conductivities are used to compute the reflection coefficients r_p of the heterostructure, that is, hBN-graphene-hBN on SiO_2/Si substrate. The resultant coefficients are used in near-field calculations based on the Lightning Rod model [55]. The calculated σ_{xx} and S_2 are plotted in Fig. S3. The reflection coefficients r_p has the following form in the near-field limit:

$$r_p(q,\omega) = 1 - \frac{\varepsilon_0}{\kappa - \frac{2\pi\sigma_{xx}}{i\omega}|q|}, \qquad q \gg \frac{\omega}{c}. \quad \text{(S2)}$$

Here ε_0 is the permittivity of vacuum, $\kappa = \varepsilon_0/\left(1 - r_p^*\right) = \kappa_1 + i\kappa_2$ is the effective permittivity of the graphene environment, and r_p^* is the reflection coefficient that the system would have in the absence of graphene. The poles of $r_p(q,\omega)$ analytically continued to complex momenta $q = q_1 + iq_2$ define the DiME dispersion. Such poles exist at $q = i\omega\kappa/2\pi\sigma_{xx}$ if $\sigma_2 > 0$ [15,54,56]. The magnetic field dependent $r_p(q)$ at $\omega = 900\ cm^{-1}$ is plotted in Fig. S4.

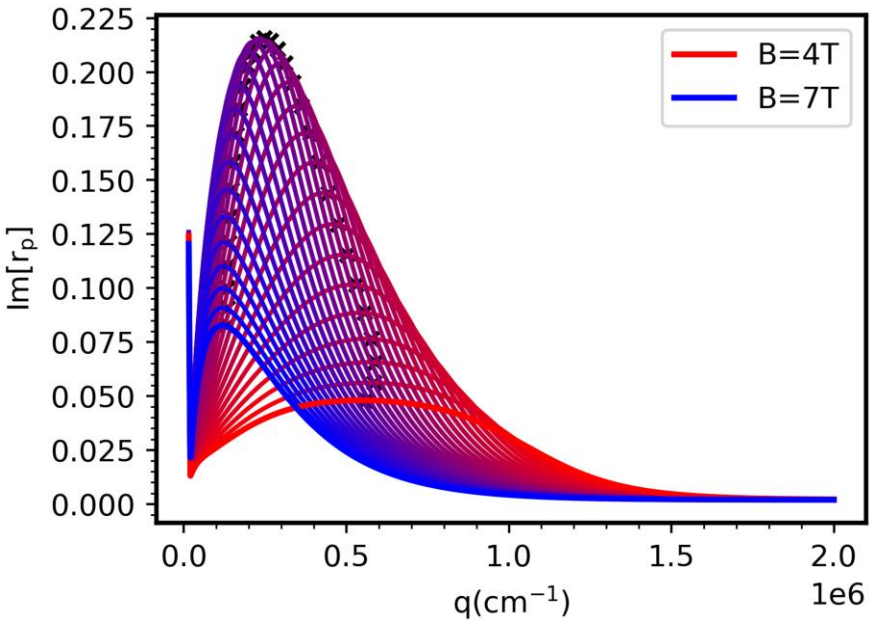

Fig.S4. *The calculated magnetic field-dependent reflection coefficient* r_p *from 4T (red) to 7T (blue). The peak position of* r_p *indicates approximately the plasmon wave vector* $q_p = 2\pi/\lambda_p$*. The width of the* r_p *indicates the Q factor of the plasmon polariton. With a typical Fermi velocity* $v_F = 1.19 \times 10^6$ *m/s and a scattering rate* $\Gamma = 8\,meV$*, the Q factor of the plasmon polariton is approximately 3 at ~110 meV, 7T, and 200K.*

S2. Gate dependence of the s-SNOM and photocurrent signals.

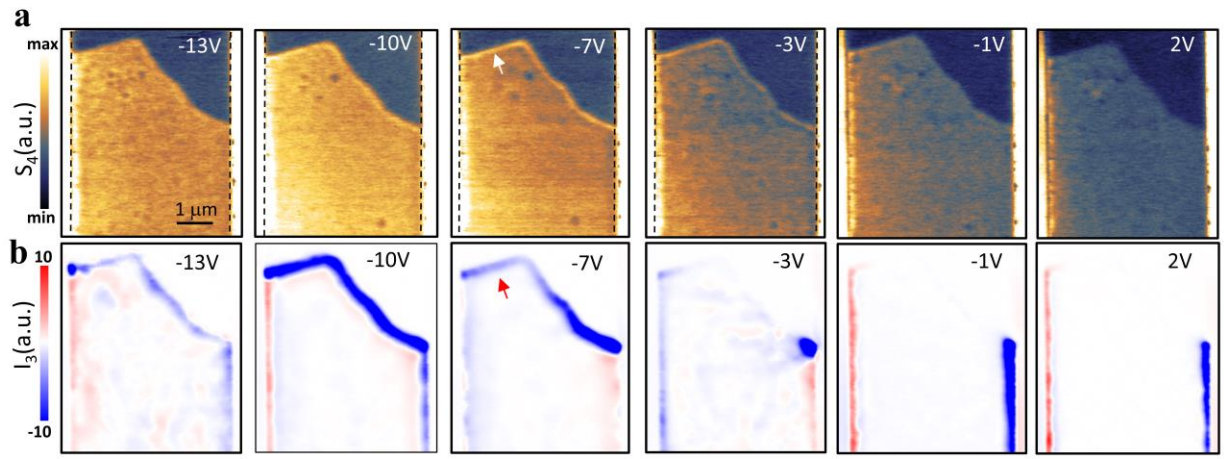

Fig.S5. *Gate-dependent near-field scattering* S_4 (***a***) *and near-field photocurrent* I_3 (***b***)*, images of the graphene edge at -6.6 T. The CNP is at around -9.5 V.*

In Fig. S5 the back-gate-dependent s-SNOM (S_4) and photocurrent (I_3) images show that when the Fermi level is increased to close to and beyond the 1st Landau level the edge DiME polariton fringe (indicated by the white arrow) and edge photocurrent (indicated by the red arrow) disappear correspondingly.

S3. Simulation of near-field photocurrent measurements

The simulation of near-field photocurrent imaging follows the Shockley-Ramo (SR) formalism [57] that has been successfully utilized to describe real-space photocurrent data in conventional far-field measurements [39,58] and near-field nano-photocurrent studies [30,31,59]. There are two kinds of current in graphene, the local photocurrent generated under the tip owing to the thermoelectric effect as $\boldsymbol{j}_{loc}(\boldsymbol{r}) = \boldsymbol{\alpha} \cdot \nabla T$, and the diffusion current due to ambient carriers driven by electrochemical potential ϕ as $\boldsymbol{j}_d = -\boldsymbol{\sigma} \cdot \nabla \phi$, where $\boldsymbol{\alpha} = \begin{bmatrix} \alpha_{xx} & \alpha_{xy} \\ -\alpha_{xy} & \alpha_{xx} \end{bmatrix}$ and $\boldsymbol{\sigma} = \begin{bmatrix} \sigma_{xx} & \sigma_{xy} \\ -\sigma_{xy} & \sigma_{xx} \end{bmatrix}$ are the dc thermoelectric conductivity matrix and dc conductivity matrix, respectively [39,57]. The total currents obey the continuity equation, so $\nabla \cdot (\boldsymbol{j}_d + \boldsymbol{j}_{loc}) = 0$.

In the SR formalism, we define the auxiliary weighting field ψ and its accompanying auxiliary current $\boldsymbol{j}_\psi = -\boldsymbol{\sigma}^T \nabla \psi$ on the graphene domain. It satisfies the Laplace equation as $\nabla \cdot \boldsymbol{j}_\psi = 0$ with the natural boundary conditions: $\boldsymbol{n} \cdot \boldsymbol{j}_\psi = 0$ at the sample-vacuum interface (non-contact edge), and $\boldsymbol{n} \times \nabla \psi = 0$ at the sample-contact interface (contact edge), where $\boldsymbol{n}$ is the unit vector normal to the boundary. In our calculation, for simplicity, ψ is set to 1 at the current-collecting contacts and 0 at the grounded contacts. The measured photocurrent I_{PC} is now related to the local photocurrent $\boldsymbol{j}_{loc}$ as:

$$I_{PC} = \iint \nabla \psi(\boldsymbol{r}') \cdot \boldsymbol{j}_{loc}(\boldsymbol{r}') d^2\boldsymbol{r}' \tag{S3}$$

Near the edge,

$$\begin{aligned} I_{PC} &= \iint \nabla \psi(\boldsymbol{r}') \cdot \boldsymbol{\alpha} \nabla T(\boldsymbol{r}') d^2\boldsymbol{r}' \\ &= \alpha_{xx} \iint \nabla \cdot (T \nabla \psi) d^2\boldsymbol{r}' + \alpha_{xy} \iint \nabla \times (T \nabla \psi) d^2\boldsymbol{r}' \\ &= \alpha_{xx} \int T \nabla \psi \cdot d\boldsymbol{n} + \alpha_{xy} T |\nabla \psi \times d\boldsymbol{n}| \end{aligned}$$

Where $\boldsymbol{n}$ is the normal vector of the boundary. At the contact edge, where $\boldsymbol{n} \times \nabla \psi = 0$, the second term is eliminated. At the non-contact edge, where $\boldsymbol{n} \cdot (\boldsymbol{\sigma}^T \nabla \psi) = 0$, $\frac{\nabla_\perp \psi'}{\nabla_\parallel \psi'} = \frac{\sigma_{xy}}{\sigma_{xx}}$. Therefore:

$$I_{PC} = \begin{cases} \alpha_{xx} \int T \nabla\psi \cdot d\boldsymbol{n}\,, & at\ the\ contact\ edge \\ \pm \dfrac{\alpha_{xx}\sigma_{xy} - \alpha_{xy}\sigma_{xx}}{\sqrt{\sigma_{xx}^2 + \sigma_{xy}^2}} \int T|\nabla\psi'|dl\,, & at\ the\ non-contact\ edge \end{cases}$$

Besides, $\boldsymbol{\sigma}$ and $\boldsymbol{\alpha}$ of graphene obey the following equation:

$$\boldsymbol{\sigma}(B) = -\int_{-\infty}^{\infty} \boldsymbol{\sigma_0}(\varepsilon, B) \frac{\partial f}{\partial \varepsilon} d\varepsilon$$

$$\boldsymbol{\alpha}(B) = \frac{1}{e} \int_{-\infty}^{\infty} \boldsymbol{\sigma_0}(\varepsilon, B) \frac{\partial f}{\partial T} d\varepsilon$$

Where f is Fermi-Dirac distribution, $\boldsymbol{\sigma_0}(\varepsilon, B)$ is the electrical conductivity tensor of the charge carriers at energy ε on the external perpendicular magnetic field, which can be calculated with Eqs. (3.11- 3.15) from [60].

We calculate $\boldsymbol{\alpha}$ and $\boldsymbol{\sigma}$ as the magnetic field is swept from -7T to 7T at 200K using a scattering rate of 8 meV, a Fermi velocity of 1.19×10^6 m/s, a chemical potential of 20 meV, as graphene is close to the charge-neutral point but possibly still with a small offset. The dependence of diagonal and off-diagonal components of $\boldsymbol{\alpha}$ and $\boldsymbol{\sigma}$ on the magnetic field is plotted in Fig. S6.

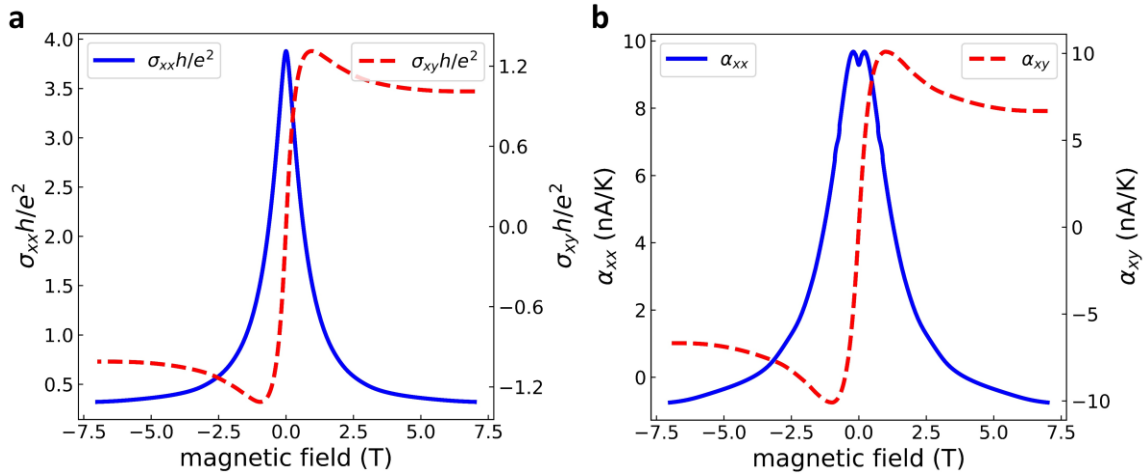

Fig.S6. *Calculated electrical and thermoelectrical conductivity for T = 200 K, impurity scattering rate = 8 meV, Fermi velocity =* 1.19×10^6 *m/s, and gap energy = 0 meV.* ***a,*** *The calculated field-dependent diagonal (σ_{xx}, blue curve, left axis) and off-diagonal (σ_{xy}, red curve, right axis) electrical conductivity of graphene.* ***b,*** *The calculated field-dependent diagonal (α_{xx}, blue curve, left axis) and off-diagonal (α_{xy}, red curve, right axis) thermoelectrical conductivity of graphene.*

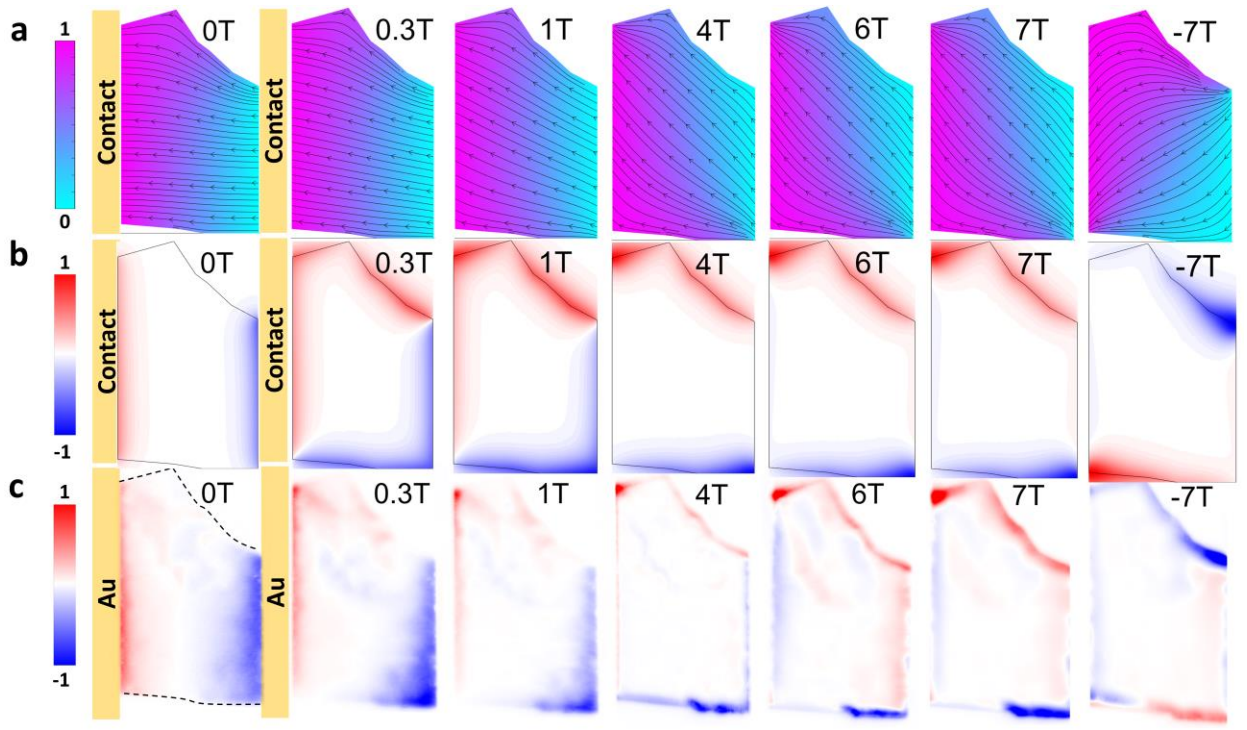

Fig.S7. *Comparison between simulated and experimental photocurrent mappings.* ***a****, calculated field-dependent auxiliary weighting field* ψ *(colormap) and auxiliary current* j_ψ *(streamlines).* ***b,c,*** *Simulated (****b****) and experimental (****c****) (from Fig. 2b) photocurrent* I_{PC} *map. The gold contacts are only shown in the first panel in each column.*

Using the calculated $\boldsymbol{\alpha}(B)$ and $\boldsymbol{\sigma}(B)$, we calculated the auxiliary weighting field ψ (Fig. S7a colormap), auxiliary current $\boldsymbol{j}_\psi$ (Fig. S7a streamlines) and photocurrent (Fig. S7b) for the two-terminal graphene device as seen in the experiment, whose left and right edges contact the gold electrodes, and the top and bottom edges are free of contacts.

In zero magnetic field, where $\sigma_{xy} = 0$ and $\alpha_{xy} = 0$ (see Fig. S6), $\boldsymbol{j}_\psi$ is parallel to the non-contact graphene edge and the photocurrent near the free boundary vanishes according to Eq. 2. As the magnetic field increases, α_{xx} decreases and σ_{xy} becomes nonzero (see Fig. S6), hence the contacted edge photocurrent fades out while the non-contact edge photocurrent emerges. With increasing fields, the streamlines of $\boldsymbol{j}_\psi$ start to orient diagonally across the graphene sheet, so that the photocurrent is locally enhanced at two opposite corners. As B sweeps from ± 4 T to ± 7 T, the photocurrent pattern close to the non-contacted edge has no significant change because of the slowly varying σ_{xy} and α_{xy}. In addition, σ_{xy} switches sign with opposite magnetic fields. Correspondingly, the photocurrent hot spots move to the other pair of corners.

We attribute the disagreement between the calculation and experiment at the bottom-left corner to the defects in graphene. We note that the simulated photocurrent near the non-contacted edge is not as strong as the one in experiments at ± 7 T since we do not include Landau transition-enhanced light absorption in the simulation.

Supplementary Information References

52. Li, Z. Q. *et al.* Infrared probe of the anomalous magnetotransport of highly oriented pyrolytic graphite in the extreme quantum limit. *Phys Rev B* **74**, 195404 (2006).

53. Yumoto, G., Matsunaga, R., Hibino, H. & Shimano, R. Ultrafast Terahertz Nonlinear Optics of Landau Level Transitions in a Monolayer Graphene. *Phys Rev Lett* **120**, 107401 (2018).

54. Nedoliuk, I. O., Hu, S., Geim, A. K. & Kuzmenko, A. B. Colossal infrared and terahertz magneto-optical activity in a two-dimensional Dirac material. *Nature Nanotechnology* vol. 14 756–761 Preprint at https://doi.org/10.1038/s41565-019-0489-8 (2019).

55. Bouhelier, A. Field-enhanced scanning near-field optical microscopy. *Microscopy Research and Technique* vol. 69 563–579 Preprint at https://doi.org/10.1002/jemt.20328 (2006).

56. Walsh, B. M., Foster, J. C., Erickson, P. J. & Sibeck, D. G. Tunable Phonon Polaritons in Atomically Thin van der Waals Crystals of Boron Nitride. *Science (1979)* **343**, 1122–1125 (2014).

57. Song, J. C. W. & Levitov, L. S. Shockley-Ramo theorem and long-range photocurrent response in gapless materials. *Phys Rev B* **90**, 75415 (2014).

58. Ma, Q. *et al.* Giant intrinsic photoresponse in pristine graphene. *Nature Nanotechnology* vol. 14 145–150 Preprint at https://doi.org/10.1038/s41565-018-0323-8 (2019).

59. Hesp, N. C. H. *et al.* Nano-imaging photoresponse in a moiré unit cell of minimally twisted bilayer graphene. *Nat Commun* **12**, (2021).

60. Gusynin, V. P. & Sharapov, S. G. Transport of Dirac quasiparticles in graphene: Hall and optical conductivities. (2006) doi:10.1103/PhysRevB.73.245411.